



HAL
open science

Thermally activated domain wall motion in [Co/Ni](111) superlattices with perpendicular magnetic anisotropy

S. Le Gall, N. Vernier, F. Montaigne, M. Gottwald, D. Lacour, M. Hehn, D. Ravelosona, S. Mangin, S. Andrieu, Thomas Hauet

► To cite this version:

S. Le Gall, N. Vernier, F. Montaigne, M. Gottwald, D. Lacour, et al.. Thermally activated domain wall motion in [Co/Ni](111) superlattices with perpendicular magnetic anisotropy. *Applied Physics Letters*, 2015, 106 (6), pp.062406. 10.1063/1.4908177 . hal-01246638

HAL Id: hal-01246638

<https://hal.science/hal-01246638>

Submitted on 12 Mar 2020

HAL is a multi-disciplinary open access archive for the deposit and dissemination of scientific research documents, whether they are published or not. The documents may come from teaching and research institutions in France or abroad, or from public or private research centers.

L'archive ouverte pluridisciplinaire **HAL**, est destinée au dépôt et à la diffusion de documents scientifiques de niveau recherche, publiés ou non, émanant des établissements d'enseignement et de recherche français ou étrangers, des laboratoires publics ou privés.



Thermally activated domain wall motion in [Co/Ni](111) superlattices with perpendicular magnetic anisotropy

S. Le Gall, N. Vernier, F. Montaigne, M. Gottwald, D. Lacour, M. Hehn, D. Ravelosona, S. Mangin, S. Andrieu, and T. Hauet

Citation: *Applied Physics Letters* **106**, 062406 (2015); doi: 10.1063/1.4908177

View online: <http://dx.doi.org/10.1063/1.4908177>

View Table of Contents: <http://scitation.aip.org/content/aip/journal/apl/106/6?ver=pdfcov>

Published by the [AIP Publishing](#)

Articles you may be interested in

[Annealing effect and under/capping layer study on Co/Ni multilayer thin films for domain wall motion](#)

J. Appl. Phys. **113**, 17C116 (2013); 10.1063/1.4795720

[Magnetic field insensitivity of magnetic domain wall velocity induced by electrical current in Co/Ni nanowire](#)

Appl. Phys. Lett. **98**, 192509 (2011); 10.1063/1.3590713

[Large thermal stability independent of critical current of domain wall motion in Co/Ni nanowires with step pinning sites](#)

J. Appl. Phys. **108**, 113914 (2010); 10.1063/1.3518046

[Relation between critical current of domain wall motion and wire dimension in perpendicularly magnetized Co/Ni nanowires](#)

Appl. Phys. Lett. **95**, 232504 (2009); 10.1063/1.3271827

[Effect of \[111\] texture on the perpendicular magnetic anisotropy of Co/Ni multilayers](#)

J. Appl. Phys. **84**, 3273 (1998); 10.1063/1.368482

A banner for Applied Physics Letters featuring the journal's logo and the text 'Meet The New Deputy Editors'. Below the text are three circular headshots of the new deputy editors: Alexander A. Balandin, Qing Hu, and David L. Price.

AIP | Applied Physics Letters

Meet The New Deputy Editors

 Alexander A. Balandin

 Qing Hu

 David L. Price

Thermally activated domain wall motion in [Co/Ni](111) superlattices with perpendicular magnetic anisotropy

S. Le Gall,^{1,2,a)} N. Vernier,³ F. Montaigne,¹ M. Gottwald,¹ D. Lacour,¹ M. Hehn,¹ D. Ravelosona,³ S. Mangin,¹ S. Andrieu,¹ and T. Hauet^{1,b)}

¹Institut Jean-Lamour, UMR-CNRS 7198, Université de Lorraine, Nancy, France

²Génie Electrique et Electronique de Paris, UMR-CNRS 8507, SUPELEC, Univ. Paris-Sud XI, UPMC Paris VI, 11 rue Joliot Curie, Plateau de Moulon, F-91192 Gif-sur-Yvette Cedex, France

³Institut Electronique Fondamentale, UMR-CNRS 8622, Univ. Paris-Sud XI, Orsay, France

(Received 10 November 2014; accepted 3 February 2015; published online 11 February 2015)

Field-induced magnetization dynamics in a [Co/Ni] superlattice exhibiting strong perpendicular magnetic anisotropy is studied using Kerr microscopy. We report domain wall velocity over 8 decades within thermally activated, transitory, and flow dynamical regimes. At low field, the thermally activated regime is characterized by dendritic domain growth that differs from the creep mechanism usually observed for the interaction of domains wall with a 2D random pinning potential for layers grown by sputtering. This result is explained by the epitaxial nature of the [Co/Ni] superlattices involving a single-type defect. The transition from the thermally activated to the flow regime is characterized by a reduction of the density of non-reversed domains which exists after domain wall displacement. © 2015 AIP Publishing LLC. [<http://dx.doi.org/10.1063/1.4908177>]

The control of magnetic domain wall (DW) motion under the action of an electrical current is of great interest for the development of new data storage electronic devices such as magnetic racetrack memories¹ or logic devices.² In this context, materials with perpendicular magnetic anisotropy (PMA) are particularly attractive,^{3,4} since they exhibit very narrow domain walls compatible with high density storage as well as spin-orbits effect that can improve the efficiency of current-induced domain wall motion.^{5,6} However, even if the efficiency of current driven DW motion can be enhanced, the threshold current is still limited by the presence of structural defects in the materials. Particularly, the strong interaction of narrow DWs with random nanoscale inhomogeneities can lead to a so-called thermally activated creep motion for $H \ll H_{\text{dep}}$, where H_{dep} is the depinning field. This creep regime has been observed in various ultra thin films with PMA such as, for instance, Co/Pt,^{7,8} CoFe, or CoFeB.⁹ Particularly, a $\ln(v)$ versus $H^{-1/4}$ dependence has been found consistent with the propagation of a 1D domain wall in a 2D weak random disorder. As these films are usually deposited by sputtering, the random disorder originates in particular, from crystalline texture, interface intermixing, or grain boundaries, which induce a distribution of PMA on the nanoscale. In epitaxial systems, the nature, density, and distribution of structural inhomogeneities can be very different, which may give rise to a different mechanism of domain wall motion. This has been shown, for example, in L_{10} FePt films with PMA¹⁰ where extended 3D microtwins induced by a relaxation process generate a dendritic like motion distinct from the creep mechanism.

Along this line of developing efficient materials for racetrack memories devices, [Co/Ni] multilayer^{11,12} shows very good promise since low propagation fields¹¹ and large

spin-orbit effect have been evidenced in (111) textured films.⁶ Recently, we have successfully grown single-crystal [Co/Ni] (111) superlattices by molecular beam epitaxy (MBE).^{13,14} Monoatomic control of the successive Co and Ni layers has allowed us to tune very precisely the PMA. Moreover, epitaxial [Co/Ni](111) shows a low damping constant down to 0.02 measured by ferromagnetic resonance (see Ref. 15 for Co/Ni multilayers), enhanced spin moment,¹⁴ and high spin polarization at the Fermi level compared to bulk Co.¹⁶ Thus, these epitaxial MBE-grown [Co/Ni](111) superlattices appear as model systems to further understand the role of structural inhomogeneities on the physics of DW dynamics.

In this letter, we investigate the magnetization dynamics in epitaxial [Co/Ni](111) layer. Kerr microscopy imaging shows that the Co/Ni full films have little nucleation point density slightly below the coercivity field. The field induced magnetization reversal through domain wall motion is analyzed and linked to three DW velocity regimes. The thermally activated regime found at low field differs from the creep regime usually observed for sputtered systems^{7,17} and its specificities are correlated to the epitaxial nature of our Co/Ni films. We clearly show that depending on the DW velocity regime the density of unreversed domain left after “saturation” is drastically different which can have a strong effect on macroscopic hysteresis loop.

Epitaxial $V(5)/\text{Au}(1)/\text{Ni}(0.2)/[\text{Co}(0.5)/\text{Ni}(0.6)]_{\times 3}/\text{Au}(1.2)$ stack (thicknesses in nanometer) was deposited on sapphire (11–20) substrate by MBE under ultra-high vacuum has previously described in Ref. 13. The crystalline structure and the layer-by-layer growth have been checked during deposition using RHEED. A saturation magnetization $M_S = 9.3 \times 10^5$ A/m (930 emu/cm^3) and an effective anisotropy constant $K_{\text{eff}} = 3.0 \times 10^5 \text{ J/m}^3$ ($3 \times 10^4 \text{ ergs/cm}^3$) were determined with a commercial SQUID-VSM magnetometer. The magnetization reversal was studied by magneto-optical Kerr effect (MOKE) microscopy at room temperature (RT). The magnetization reversal

^{a)}Author to whom correspondence should be addressed. Electronic mail: sylvain.le-gall@u-psud.fr.

^{b)}Thomas.Hauet@univ-lorraine.fr

under DC applied magnetic field in a continuous film is presented in Fig. 1. The Kerr loop measured over large $2.6 \times 4 \text{ mm}^2$ area shows a coercivity $\mu_0 H_c = 22.5 \text{ mT}$ (Fig. 1(a)). To investigate the nucleation processes, images are taken for magnetic field applied slightly below the coercive field as shown in Fig. 1(b) for $H = 21.1 \text{ mT}$. In those conditions, the [Co/Ni] superlattice shows only few nucleation sites per mm^2 . In Fig. 1(b), there are 7 nucleation spots (black areas) for a 10 mm^2 area. Nucleation spots are generally related to local variations of magnetocrystalline anisotropy or magnetization. In regular sputtered PMA multilayers, anisotropy variation is found to mainly arise from crystalline misorientation.^{18,19} In epitaxial film, such granular structure does not exist but some other defects can affect the magnetic anisotropy such as twin domains and stacking fault as discussed below in more details.

On the same film, the DW velocity was determined by measuring the DW displacement from a nucleation spot after application of 5 ms to $5 \mu\text{s}$ magnetic field pulses (H_{pulse}). Figure 2 gives the DW velocity as a function of $\mu_0 H_{\text{pulse}}$ (the scale of the DW velocity is linear in (a) and logarithmic in (b)). Three different regimes can be observed: for fields lower than 24 mT , the DW velocity exponentially increases with the field amplitude, for fields higher than 27 mT , the velocity saturates around 10 m/s , whereas between 24 and 27 mT , a transitional regime occurs. The magnetic configurations after the domain growth have been studied for the three regimes and are shown for magnetic fields of 23.7 , 25.6 , and

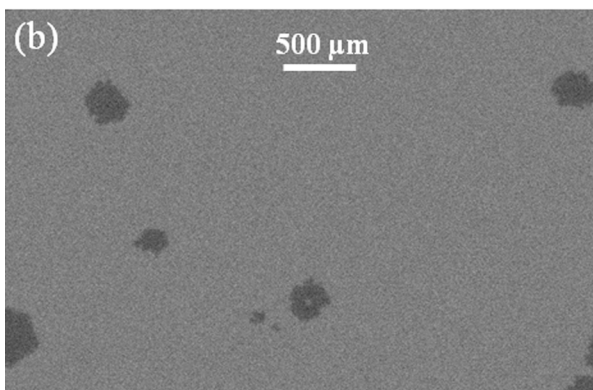
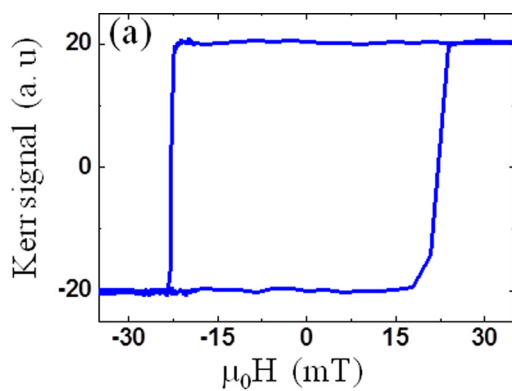


FIG. 1. Magnetization reversal under DC magnetic field done at RT on a $2.6 \times 4 \text{ mm}^2$ area [Co/Ni](111) superlattice full film using Kerr microscopy experiment. (a) Kerr-magnetometry: hysteresis loop (coercivity: $\mu_0 H_c = 22.5 \text{ mT}$). (b) Kerr-imaging: picture taken an applied DC $\mu_0 H = 21.1 \text{ mT}$. The black magnetic contrast is related to reversed magnetization for $H > 0$, and the grey one being the unreversed part obtained after saturation at a higher opposite field (around -500 mT).

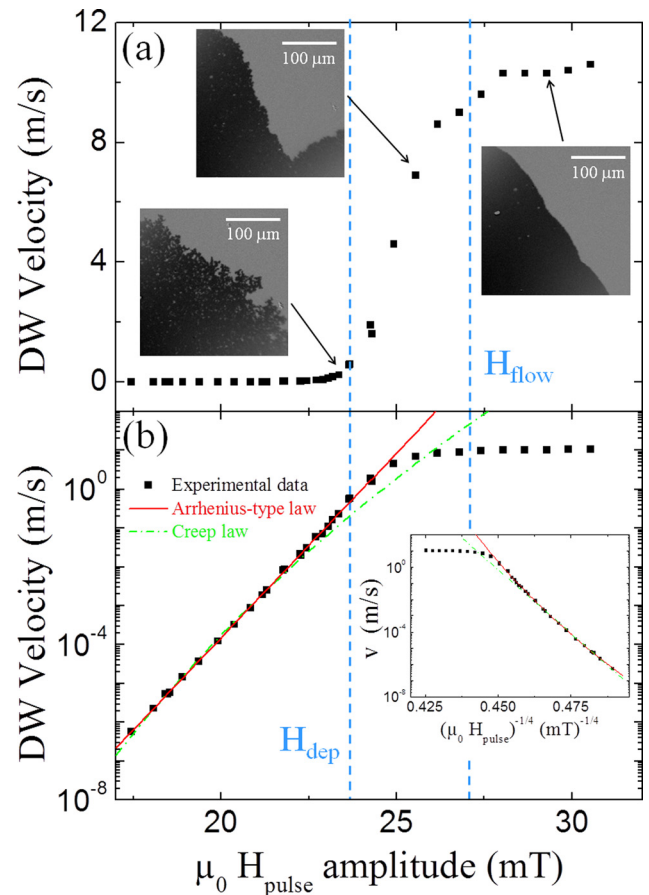


FIG. 2. DW velocity measured for the full film at RT as a function of the pulsed magnetic field intensity ($5 \mu\text{s}$ – 5 ms). (a) Linear scale. (b) Semi-logarithmic scale. Kerr microscopy pictures of the magnetic domain after DW propagation for 23.7 , 25.6 , and 29.3 mT are added ($275 \times 275 \mu\text{m}^2$ area). The red solid line is an Arrhenius-type law fit, and the green dashed line is the fit for creep law. Inset Fig. 2(b): Velocity vs $(\mu_0 H_{\text{pulse}})^{-1/4}$ representation.

29.3 mT , respectively, in Fig. 2(a). A correlation between the regimes of DW velocity and the mechanism of domain growth is clearly identified. Indeed for $\mu_0 H_{\text{pulse}} = 23.7 \text{ mT}$, the domain has expanded through dendritic-growth,²⁰ leaving some unreversed spots behind the domain boundary.^{21,22} The domain growth transits from dendritic to wall-front motion regime²¹ where the number of residual unreversed sites decreases as can be seen for 25.6 and 29.3 mT . Note that some residual domains persist up to 31 mT (the maximum field that we could reach).

In the following, we focus on the three DW velocity regimes. At low fields for ultra-thin magnetic films with PMA, as discussed above,^{7–9,17} a creep regime²³ is usually expected. In that case, the interaction of a 1D domain walls with a 2D random disorder leads to DW velocity given by $v(H) = v_0 \exp[-U_C (H_{\text{dep}}/H)^{1/4}/k_B T]$, where v_0 is the prefactor, U_C is a characteristic energy barrier, k_B is the Boltzmann constant, T is the temperature, and H_{dep} is the depinning field. In Fig. 2(b) and in the inset of Fig. 2(b), we clearly observe that the creep law does not fit well the data above magnetic fields of 21 mT . Instead, the experimental data fit better with $v(H) = v_0 \exp[2\mu_0 M_S V_a (H - H_{\text{dep}})/k_B T]$ (called Arrhenius-type law of Fig. 2), where v_0 is the prefactor and V_a is the activation volume.²⁴ The $\ln(v)$ versus $\mu_0 H_{\text{pulse}}$ is

linear over 7 decades of magnitude up to the depinning field $\mu_0 H_{\text{dep}} = 24 \text{ mT}$ (i.e., the field at which the DW leaves the thermally activated regime). The slope of $\ln(v)$ versus $\mu_0 H_{\text{pulse}}$ gives $2M_S V_a / k_B T = 2190 \text{ J/T}$, which leads to an activation volume $V_a = 4900 \text{ nm}^3$. It allows us to determine a characteristic propagation length $\xi = (V_a / t_{\text{Co/Ni}})^{1/2}$ around 37 nm , which corresponds to the length scale of the pinning potential. Considering $\mu_0 H_{\text{dep}} = 24 \text{ mT}$, the depinning energy barrier $E_{\text{dep}} = 2M_S V_a \mu_0 H_{\text{dep}}$ is thus found to be around $53 \text{ k}_B T$ at RT, which is much larger than that of Co ($4 \text{ k}_B T$)²⁴ or FePt ($27 \text{ k}_B T$).²⁵

The fact that no creep regime is observed relies on the nature of the pinning defects in our epitaxial Co/Ni multilayers. Particularly, the data are consistent with the presence of a single type defect²⁵ instead of a distribution of different structural inhomogeneities. For the epitaxial [Co/Ni] system, a regular single-type defect pattern is consistent with magnetization reversal zone by zone as observed by MOKE imaging consistent with random-walk along the defect network.^{26,27} A correlation between fractal dendritic-growth and defects (microtwin) is also highlighted on high coercivity epitaxial FePt system and has been analyzed as percolation in a band lattice.¹⁰ In our case, we have identified two types of defect in the superlattice films that could affect domain wall motion, but we cannot claim which one contributes to the unique energy barrier. The first is due to the formation of twin domains in the V buffer layer as shown by RHEED since the epitaxial relationships of V $[-111]$ parallel to $\alpha\text{-Al}_2\text{O}_3$ $[0001]$ and V $[-11-1]$ parallel to $\alpha\text{-Al}_2\text{O}_3$ $[0001]$ are equivalent. It affects the Au layer and further forms grain boundary defects in the Co/Ni layer. The twin domain boundary period is expected to be of the order of 100 nm or less. The second type of observed defect consists in stacking faults in the Co/Ni film itself. Locally A-B-C pile can be replaced by A-B-A pile, for instance. Also, grain boundaries have actually been observed by transmission electron microscopy. It was, however, very difficult to get information about the average distance between grain boundaries due to this second type of defect. Using Au(111) single crystal as substrate would cancel twin domains and would allow to disentangle the role of twin domains from other sources of pinning.

For magnetic fields higher than H_{dep} (Fig. 2(a)), DW velocity enters in a viscous flow regime⁷ where two regimes can be distinguished without Walker breakdown. Considering the 1D DW model,²⁸ it is predicted a steady and a precessional linear regime separated by the Walker field $H_w = \alpha M_S N_y / 2$,²⁹ where N_y is the demagnetizing factor across the wall. Due to the low damping constant α in epitaxial [Co/Ni], the estimated $\mu_0 H_w$ is about 10 mT which is much lower than the depinning field H_{dep} . Therefore, H_w lies inside the thermally activated regime and the Walker breakdown is hidden as in the case of CoFeB/MgO.⁹ For $H_{\text{dep}} < H < H_{\text{flow}}$, the transitory regime is usually called depinning regime⁷ because it separates thermally activated behavior to flow. The slope between $\mu_0 H_{\text{dep}} = 24 \text{ mT}$ and upper limit estimated to $\mu_0 H_{\text{flow}} = 27 \text{ mT}$ gives a value around $3.7 \text{ m s}^{-1}/\text{mT}$. This transitory regime also marks the transition between dendritic growth and wall-motion. For $H > H_{\text{flow}}$, the velocity seems to reach a plateau for around

10 m/s . The velocity plateau agrees well with other studies.^{9,30} The flow regime velocity in Fig. 2(b) is similar to that obtained by Yamada *et al.* on sputtered [Co/Ni] multilayer for sub-micronic wire width.³⁰ The fact that MBE-grown [Co/Ni] superlattices does not show faster domain wall motion than [Co/Ni] multilayers grown by sputtering is not surprising since in the flow regime, the DW propagation is less sensitive to pinning defects and should behave as described by the 1D model. The plateau arises probably because we have reached the low mobility precessional regime after the Walker breakdown.

Magnetic domain imaging, achieved using the magneto-optical Kerr effect, is found to be a great tool to study the magnetization dynamic. In the following, we focus on the dendritic behavior of DW motion, which is characterized by non-reversed regions. In a previous study, cumulative minor loops growth in PMA multilayers was observed³¹ and could be explained as an accumulation of small unreversed domains that then act as nucleation center that aid subsequent reversals and facilitate the “cumulative minor loop growth” effect. The nucleation process and the nature of the interaction between the domain walls and the extended defect structure remain open questions.³² To get a better understanding of the presence of non-reversed domains, we performed Kerr microscopy experiments using a specific procedure described as follow: after full saturation of magnetization using a field of -50 mT (step 1), a constant DC field of $\mu_0 H = 20 \text{ mT}$ is applied to expand the reversed domain propagating from the nucleation site (see Fig. 1(b)). The field is stopped when DW is in the camera’s view. Step 2 consists of the application of a single pulsed field whose amplitude varies between 23.9 and 31 mT (the duration depends of the field amplitude). As the size of the non-reversed spots is very small (close or below the resolution of the instrument), an opposite DC field of $\mu_0 H = -17 \text{ mT}$ is applied during several seconds in order to extend the non-reversed domains and make them more visible (step 3). We have checked that for -17 mT , no new nucleation processes occur. Magnetic images at steps 1 and 3 are shown in Fig. 3(a) for $\mu_0 H_{\text{pulse}} = 25.2, 26,$ and 28.1 mT , respectively. The transition between the two regions corresponding to DC $\mu_0 H = 20 \text{ mT}$ and $\mu_0 H_{\text{pulse}}$ is highlighted by a yellow line in Fig. 3.

The density of unreversed domains for the region where the propagation occurs only under field pulsed (zone 2) is plotted as a function of $\mu_0 H_{\text{pulse}}$ in Fig. 3(b). For magnetic field lower than 26 mT , the density of non-reversed domains (about 8000 spots by mm^2) does not vary significantly with $\mu_0 H_{\text{pulse}}$. This field range corresponds to the transition between dendritic-growth and wall motion behavior for DW dynamics and is close to H_{flow} . For a field pulse larger than 26 mT , the density decreases drastically and goes to zero at $\mu_0 H_{\text{pulse}} = 31 \text{ mT}$. The viscous flow regime is then only reached at this stage. This demonstrates that the type of domain reversal regime determines the number of nucleation center which can greatly affect the macroscopic hysteresis loop.³¹ The nature and the initial size of the remaining domain could not be studied with our experimental technique. In Ref. 33, it has been shown that a DW can circumvent a defect by propagating around it, which generates two parallel

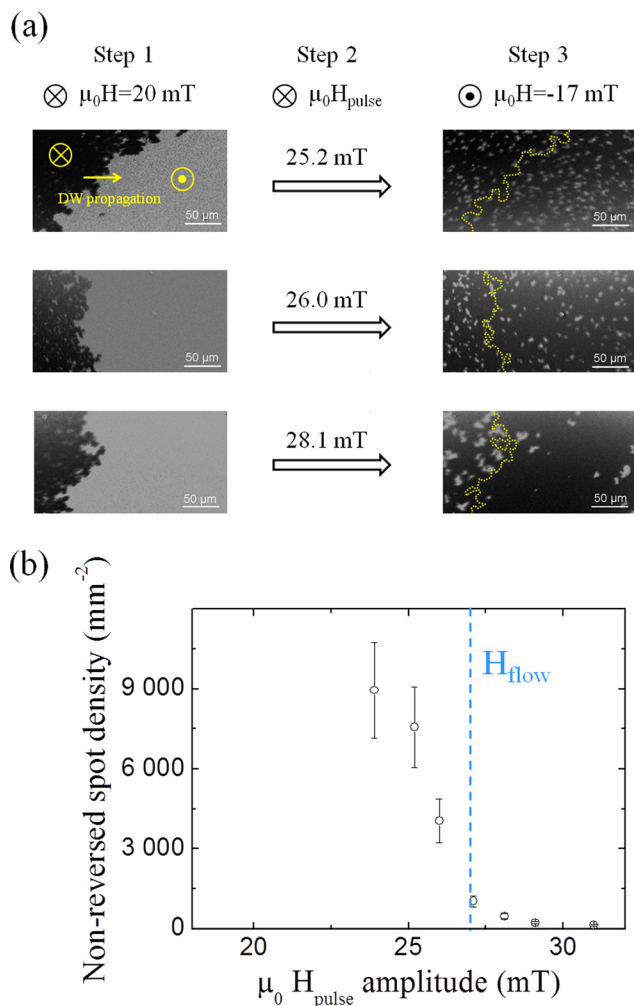


FIG. 3. Non-reversed micro-domains analysis (a) pictures on the left are the view of the non-reversed spot during DW propagation. The yellow dashed line indicates the originate DW position after propagation under DC $\mu_0 H = 20$ mT, moving direction from left to right. Note that the size of the non-reversed spot can be changed from one run to another due to duration (between 7 and 14 s) of opposite field of -17 mT. (b) Non-reversed spot density as a function of $\mu_0 H_{\text{pulse}}$ for zone 2 (right side on pictures 3(a)). The error bars are taken at 20% of the density.

domain walls. If the applied field is too low, dipolar repulsion can prevent DWs annihilation, which gives rise to 360° domain walls.³³ In the present case, no 360° DWs have been observed. Just after the annihilation, a very small closed unreversed domain is created around the defect. For such a reversed domain surrounded by an opposite magnetization, the demagnetizing field is much larger than the one obtained for 360° domain walls, so the unreversed spot can survive. Once formed, these unreversed spots become very stable and difficult to reverse due to dipolar field (many unreversed spots remain in the left side of the yellow line at the end of step 3 in Fig. 3(a)). For a circular domain, we can estimate the dipolar field on the center of the spot using $\mu_0 H_{\text{dip}} = \mu_0 t_{\text{Co/Ni}} M_S / r$, where r is the radius of the spot and $t_{\text{Co/Ni}} = 3.5$ nm is the thickness of the magnetic layer. Using this calculation, an applied field of 31 mT is needed to compensate the dipolar field of an unreversed domain larger than 260 nm of diameter.

In conclusion, we have studied field-induced DW motion in a model system based on [Co/Ni] superlattices

with large PMA. The epitaxial nature of the films allows us to observe a regime of thermally activated dendritic domain wall motion involving a barrier that changes linearly as a function of the applied magnetic field, which is different from the creep regime usually found in thin films with PMA. The propagation can be understood as a reversal zone by zone on a network of structural defects with a presence of unique energy barrier. Two types of defects are proposed, one induced by the buffer layer and the other one inside the Co/Ni multilayer. Using single Au(111) single crystal as substrate could allow to conclude on the role of the first defect. The transition to the flow regime is found to be related to the external magnetic field by overcoming the dipolar field stabilizing the unreversed regions. Our results confirm that magnetic imaging is required to properly understand the domain wall motion mechanism, especially for implementation into nanostructured spintronics devices.

We would like to thank V. Jeudy and A. Thiaville for fruitful discussions. This work was financially supported by the ANR “Friends” the Partner University Fund (France embassy), FEDER France, the Region Lorraine, and the Grand Nancy.

- ¹S. S. P. Parkin, M. Hayashi, and L. Thomas, *Science* **320**, 190 (2008).
- ²D. A. Allwood, G. Xiong, C. C. Faulkner, D. Atkinson, D. Petit, and R. P. Cowburn, *Science* **309**, 1688 (2005).
- ³S. Mangin, D. Ravelosona, J. A. Katine, M. J. Carey, B. D. Terris, and E. E. Fullerton, *Nat. Mater.* **5**, 210 (2006).
- ⁴S. Le Gall, J. Cucchiara, M. Gottwald, C. Berthelot, C.-H. Lambert, Y. Henry, D. Bedau, D. B. Gopman, H. Liu, A. D. Kent, J. Z. Sun, W. Lin, D. Ravelosona, J. A. Katine, E. E. Fullerton, and S. Mangin, *Phys. Rev. B* **86**, 014419 (2012).
- ⁵A. Thiaville, S. Rohart, E. Jué, V. Cros, and A. Fert, *Europhys. Lett.* **100**, 57002 (2012).
- ⁶K.-S. Ryu, S.-H. Yang, L. Thomas, and S. S. P. Parkin, *Nat. Commun.* **5**, 3910 (2014).
- ⁷P. J. Metaxas, J. P. Jamet, A. Mougin, M. Cormier, J. Ferré, V. Baltz, B. Rodmacq, B. Dieny, and R. L. Stamps, *Phys. Rev. Lett.* **99**, 217208 (2007).
- ⁸J.-C. Lee, K.-J. Kim, J. Ryu, K.-W. Moon, S.-J. Yun, G.-H. Gim, K.-S. Lee, K.-H. Shin, H.-W. Lee, and S.-B. Choe, *Phys. Rev. Lett.* **107**, 067201 (2011).
- ⁹C. Burrowes, N. Vernier, J.-P. Adam, L. Herrera Diez, K. Garcia, I. Barisic, G. Agnus, S. Eimer, J.-V. Kim, T. Devolder, A. Lamperti, R. Mantovan, B. Oeckert, E. E. Fullerton, and D. Ravelosona, *Appl. Phys. Lett.* **103**, 182401 (2013).
- ¹⁰J.-P. Attané, Y. Samson, A. Marty, J. C. Toussaint, G. Dubois, A. Mougin, and J.-P. Jamet, *Phys. Rev. Lett.* **93**, 257203 (2004).
- ¹¹C. Burrowes, A. P. Mihai, D. Ravelosona, J.-V. Kim, C. Chappert, L. Vila, A. Marty, Y. Samson, F. Garcia-Sanchez, L. D. Buda-Prejbeanu, I. Tudosa, E. E. Fullerton, and J.-P. Attané, *Nat. Phys.* **6**, 17 (2010).
- ¹²T. Koyama, D. Chiba, K. Ueda, K. Kondou, H. Tanigawa, S. Fukami, T. Suzuki, N. Ohshima, N. Ishiwata, Y. Nakatani, K. Kobayashi, and T. Ono, *Nat. Mater.* **10**, 194 (2011).
- ¹³S. Girod, M. Gottwald, S. Andrieu, S. Mangin, J. McCord, E. E. Fullerton, J.-M. L. Beaujour, B. J. Krishnatreya, and A. D. Kent, *Appl. Phys. Lett.* **94**, 262504 (2009).
- ¹⁴M. Gottwald, S. Girod, S. Andrieu, and S. Mangin, *IOP Conf. Ser.: Mater. Sci. Eng.* **12**, 012018 (2010).
- ¹⁵J.-M. L. Beaujour, W. Chen, K. Krycka, C.-C. Kao, J. Z. Sun, and A. D. Kent, *Eur. Phys. J. B* **59**, 475 (2007).
- ¹⁶T. Hauet, M. Gottwald, A. Neggache, A. Rajanikanth, F. Montaigne, S. Mangin, F. Bertran, P. Le Fèvre, F. Gimbert, L. Calmels, and S. Andrieu, private communication.
- ¹⁷C. Burrowes, D. Ravelosona, C. Chappert, S. Mangin, E. E. Fullerton, J. A. Katine, and B. D. Terris, *Appl. Phys. Lett.* **93**, 172513 (2008).

- ¹⁸T. Hauet, O. Hellwig, S. H. Park, C. Beigne, E. Dobisz, B. D. Terris, and D. Ravelosona, *Appl. Phys. Lett.* **98**, 172506 (2011).
- ¹⁹B. Pfau, C. M. Guenther, E. Guehrs, T. Hauet, H. Yang, L. Vinh, X. Xu, D. Yaney, R. Rick, S. Eisebitt, and O. Hellwig, *Appl. Phys. Lett.* **99**, 062502 (2011).
- ²⁰J. P. Attané, M. Tissier, A. Marty, and L. Vila, *Phys. Rev. B* **82**, 024408 (2010).
- ²¹S.-B. Choe and S.-C. Shin, *Appl. Phys. Lett.* **80**, 1791 (2002).
- ²²J. E. Davies, O. Hellwig, E. E. Fullerton, G. Denbeaux, J. B. Kortright, and K. Liu, *Phys. Rev. B* **70**, 224434 (2004).
- ²³P. Chauve, T. Giamarchi, and P. Le Doussal, *Phys. Rev. B* **62**, 6241 (2000).
- ²⁴A. Kirilyuk, J. Ferré, V. Grolier, J.-P. Jamet, and D. Renard, *J. Magn. Mater.* **171**, 45 (1997).
- ²⁵J.-P. Attané, D. Ravelosona, A. Marty, Y. Samson, and C. Chappert, *Phys. Rev. Lett.* **96**, 147204 (2006); F. Garcia-Sanchez, H. Szabolcs, A. P. Mihai, L. Vila, A. Marty, J.-P. Attané, J.-Ch. Toussaint, and L. D. Buda-Prejbeanu, *Phys. Rev. B* **81**, 134408 (2010).
- ²⁶K. B. Howard, *A Random Walk Through Fractal Dimensions*, 2nd ed. (VCH, Weinheim, 1994), Chap. 5.
- ²⁷M. Plapp and A. Karma, *Phys. Rev. Lett.* **84**, 1740 (2000).
- ²⁸N. L. Schryer and L. R. Walker, *J. Appl. Phys.* **45**, 5406 (1974).
- ²⁹A. Mougin, M. Cormier, J.-P. Adam, P. J. Metaxas, and J. Ferré, *Europhys. Lett.* **78**, 57007 (2007).
- ³⁰K. Yamada, J.-P. Jamet, Y. Nakatani, A. Mougin, A. Thiaville, T. Ono, and J. Ferré, *Appl. Phys. Express* **4**, 113001 (2011).
- ³¹A. Berger, S. Mangin, J. McCord, O. Hellwig, and E. E. Fullerton, *Phys. Rev. B* **82**, 104423 (2010).
- ³²C. Leighton, *Physics* **3**, 79 (2010).
- ³³N. Vernier, J.-P. Adam, S. Eimer, G. Agnus, T. Devolder, T. Hauet, B. Ocker, F. Garcia, and D. Ravelosona, *Appl. Phys. Lett.* **104**, 122404 (2014).